ELSEVIER

International Journal of Heat and Fluid Flow 23 (2002) 148–160

International Journal of HEAT AND FLUID FLOW

www.elsevier.com/locate/ijhff

Progress in the generalization of wall-function treatments

T.J. Craft, A.V. Gerasimov *, H. Iacovides, B.E. Launder

Mechanical Engineering Department, UMIST, Manchester M60 1QD, UK

Abstract

This paper describes progress in developing an analytical representation of the variation of the dynamic variables and temperature across the near-wall sublayer of a turbulent flow. The aim is to enable the effective "resistance" of the viscous sublayer to the transport of heat and momentum to be packaged in the form of a "wall function", thus enabling CFD predictions of convective heat transfer to be made without incurring the cost of the very fine near-wall grid that would otherwise have to be adopted. While the general idea is not new, the detailed strategy contains many new features, which have led to a scheme capable of accounting for the effects of buoyancy, pressure gradient and of variations in molecular transport properties. The scheme is applied to the problem of forced and mixed convection in a vertical pipe and to the opposed wall jet with encouraging results. © 2002 Published by Elsevier Science Inc.

1. Introduction

Virtually all CFD computations of industrial heat transfer adopt simplistic algebraic formulations to incorporate the effects of the viscous sublayer on the transport processes of interest. In that way one may avoid the huge computational penalty of employing an extremely fine grid that extends all the way to the wall. However, in commercial software, the 'wall-function' formulae adopted are of such limited applicability that accurate representation can only be relied upon in the case of near-wall turbulence in local equilibrium, a state which is far removed from those for which, in practical problems of convective heat transfer, one seeks solutions.

It must be acknowledged at the outset that these limitations were recognized from the earliest days of turbulent flow CFD. Spalding (1967), in an exhaustive account originally intended as a book, developed an elaborate set of formulae that aimed to account for modifications to the usual log-law formulae caused by pressure gradient and mass transfer through the wall as well as to circumstances where the wall function only had to account for a portion of the sublayer. The original textbook by Patankar and Spalding (1967) also incorporated similar, if somewhat less general, wall functions again incorporating effects of mass transfer and pressure gradient. This work was soon followed by a parallel treatment by Wolfshtein (1969) whose analysis was the first to incorporate the effects of high external levels of turbulence energy convected or diffused towards the wall.

Yet, these schemes, developed in the late 1960s, did not long survive but were instead replaced in CFD software by the conventional logarithmic laws for velocity and temperature, the only improvement to the original logarithmic law of Prandtl being that the friction velocity $U_\tau \equiv (\tau_{\text{wall}}/\rho)^{1/2}$ was replaced by the square-root of turbulence energy at the near-wall node, $k_P^{1/2}$.

The reasons behind this retrograde step were several. Briefly, at the level of fundamental research, wall functions were seen to be an inadequate approach for assessing conjectured transport models: for that one had to integrate to the wall and accept the computational burden imposed by the inevitable very fine grid. Moreover, even for industrial type applications it was recognized that relatively advanced wall functions did not give clearly superior results to a simple log-law formulation. There were evidently some important physical effects missing even from the elaborate forms and, in any event, none of the schemes included the effects of buoyancy.

* Corresponding author. Tel.: +44-161-200-4547; fax: +44-161-200-3723.

E-mail address: aleksey.gerasimov@stud.umist.ac.uk (A.V. Gerasimov).

0142-727X/02/$ - see front matter © 2002 Published by Elsevier Science Inc.
PII: S0142-727X(01)00143-6

There the matter has rested for three decades. There have been attempts at effectively refining the wall-function analysis (Chieng and Launder, 1980; Johnson and Launder, 1982) but still the fundamental weakness of the logarithmic velocity and temperature variations was retained. Ciofalo and Collins (1989) considered the extension of the approach to apply when the near-wall node was located in the 'buffer' region, but their elaborations have likewise not caught on.

Against this background a decision was taken at UMIST in 1999 to place a major effort into the development of improved wall functions. It was seen as intolerable that successive generations of CFD-code users should be forced to adopt wholly inadequate wall-function formulae as the only alternative to a fine grid analysis. Two entirely independent and radically different approaches have been developed. One of these, Craft et al. (2001), is based on an efficient one-dimensional numerical integration of the low-Reynolds number model of turbulence adopted. The second, described below, presents a simple analytical approach. While this strategy is ultimately less general than the numerical integration, the computational time for the same problem is some 50% less and the analysis enables one to better perceive the contribution of separate physical processes.

Section 2 explains the main assumptions adopted and the steps in the analysis for a conventional wall-function treatment while Section 3 gives the details of the proposed approach. In Section 4 we explain how this approach can be implemented within a finite-volume methodology. Then in Section 5 we present a comparison of the performance of the new wall function in two types of flows. While, as stated above, the approach is simple, the equations which emerge from the analysis are fairly intricate. For that reason many of the formulae have been transferred to appendices. In the present paper significant generalizations from taking this new wall-function approach have been achieved and demonstrated, but there remain further steps to be taken. These are briefly discussed in Section 6.

2. The conventional wall-function approach

To respond to a request from a referee, before presenting the new strategy we give the formulation adopted in a typical wall-function scenario (see Fig. 1). In such a conventional wall-function treatment:

1. The first near-wall grid node is placed far enough away from the wall at a distance y_P to be situated in the fully turbulent inner region.
2. The flow over this region is assumed to obey the inner law of the wall.
3. The local equilibrium conditions are then used to estimate the wall shear stress and also to evaluate the source terms in the turbulent transport equations (for k and other variables, depending on the model used).

Thus, in the near-wall control volume, for the velocity component parallel to the wall, the wall shear stress is commonly obtained from the following inversion and generalization of the log-law, Launder and Spalding (1974):

$$\tau_{\text{wall}} = \frac{\kappa c_\mu^{1/4} \rho k_P^{1/2} U_P}{\ln(E c_\mu^{1/4} y_P^*)}. \tag{2.1}$$

The above expression for the wall shear stress is then adopted in accounting for the forces applied to the near-wall control volume, for the momentum component parallel to the wall (see Fig. 1).

When integrating the k transport equation for the near-wall cell:

1. Viscous transport of k to the wall is neglected.
2. Because of their very rapid variation near the wall, the source terms in the k equation, P_k and ε, should not be assumed constant over the control volume as is the usual practice with the internal cells.

These two terms are instead evaluated through analytical integration. We summarize below the type of strategy conventionally adopted.

2.1. Calculation of near-wall P_k

The starting point is the assumption that in the near-wall cell turbulence energy generation is by simple shear:

$$P_k = -\rho \overline{uv} \frac{\partial U}{\partial y}. \tag{2.2}$$

From the local equilibrium conditions

$$-\rho \overline{uv} = \tau_{\text{wall}} \quad \text{and} \quad U = \frac{\tau_{\text{wall}}}{\kappa c_\mu^{1/4} \rho k_P^{1/2}} \ln\left(E \frac{y k_P^{1/2}}{\nu}\right)$$

$$\Rightarrow \quad \frac{\partial U}{\partial y} = \frac{\tau_{\text{wall}}}{\kappa c_\mu^{1/4} \rho k_P^{1/2} y}.$$

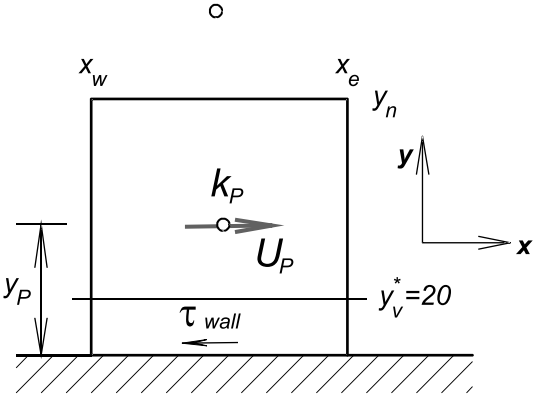

Fig. 1. Near-wall cell arrangement for conventional wall function.

Thus

$$P_k = \frac{\tau_{\text{wall}}^2}{\kappa c_\mu^{1/4} \rho k_P^{1/2} y}. \tag{2.3}$$

The above expression already contains the assumption that the turbulent shear stress remains constant over the control volume ($= \tau_{\text{wall}}$). Also, by setting k constant ($= k_P$), P_k can be integrated over the control volume. The integration is not, however, carried out over the entire control volume. The near-wall cell is subdivided into two layers: the fully turbulent region, away from the wall and the viscous layer next to the wall. P_k is assumed to be zero within the viscous layer. The edge of the sublayer is taken to be at a distance y_v from the wall, where $y_v k_P^{1/2}/\nu = 20$. Then the average P_k over the near-wall cell is obtained from

$$\overline{P_k} = \frac{1}{y_n} \int_{y_v}^{y_n} \frac{\tau_{\text{wall}}^2}{\kappa c_\mu^{1/4} \rho k_P^{1/2} y} \, \mathrm{d}y = \frac{\tau_{\text{wall}}^2}{\kappa c_\mu^{1/4} \rho k_P^{1/2} y_n} \ln\left(\frac{y_n}{y_v}\right). \tag{2.4}$$

2.2. Calculation of near-wall dissipation rate

Over the fully turbulent layer $\varepsilon = k_P^{3/2}/(c_l y)$. Within the viscous sublayer, ε is assumed to remain constant and is evaluated at the edge of the sublayer as $\varepsilon_v = k_P^{3/2}/(c_l y)$.

Integration then leads to:

$$\begin{aligned} \overline{\varepsilon} &= \frac{1}{y_n}\left[y_v \frac{k_P^{3/2}}{c_l y_v} + \int_{y_v}^{y_n} \frac{k_P^{3/2}}{c_l y} \, \mathrm{d}y \right] \\ &= \frac{1}{y_n}\left[y_v \frac{k_P^{3/2}}{c_l y_v} + \frac{k_P^{3/2}}{c_l} \ln\left(\frac{y_n}{y_v}\right) \right]. \end{aligned} \tag{2.5}$$

The transport equation for ε is not solved over the near-wall control volumes. The value of ε at the near-wall node is instead prescribed as

$$\varepsilon_P = \frac{k_P^{3/2}}{c_l y_P}. \tag{2.6}$$

3. The physical model proposed for the wall-adjacent region

3.1. Preliminaries

As in Section 2, the proposed treatment is developed with a finite-volume numerical discretization of the flow in mind. Thus Fig. 2 shows the near-wall control volume (CV) where the south boundary of the CV coincides with the wall and the cell node is at P. The viscous sublayer extends to a distance y_v from the wall and, for the present, we assume that y_n (the value of the normal coordinate at the cell face n) is greater than y_v. The turbulent viscosity is taken as zero within the viscous layer and, for $y > y_v$, is assumed to increase linearly with distance from the edge of the sublayer

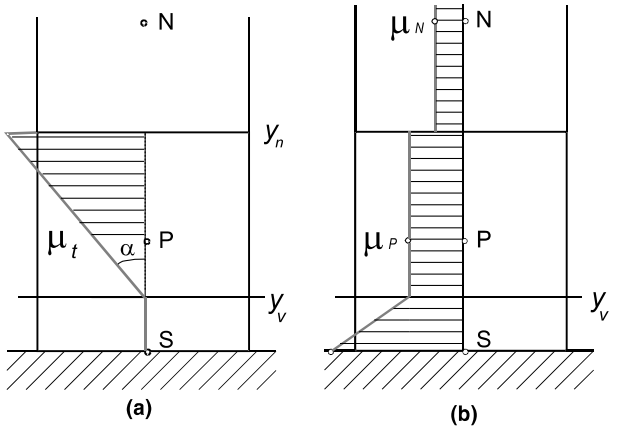

Fig. 2. (a) Turbulent viscosity variation. (b) Molecular viscosity variation.

$$\frac{\mu_t}{\mu_v} = \alpha(y^* - y_v^*) = c_\mu c_l (y^* - y_v^*). \tag{3.1}$$

The constants c_μ and c_l are the conventional ones adopted in one-equation eddy viscosity models (0.09 and 2.55) while y^* is the dimensionless wall distance $\rho_v y k_P^{1/2}/\mu_v$, where the subscript v denotes properties evaluated at the edge of the viscous sublayer. While Chieng and Launder (1980) proposed that k in the definition of y^* should also be evaluated at y_v, we have found this apparently logical choice rendered the result more sensitive to the thickness of the wall-adjacent control volume and, moreover, could greatly impair convergence of the equation set. We note that rather than a conventional damping function, Eq. (3.1) merely shifts the turbulent flow origin from the wall to the edge of the viscous layer. This choice simplifies integration, yet retains the essentials of a continuous effective viscosity curve where the turbulent viscosity is zero for a finite region next to the wall. As Fig. 2(b) suggests, a uniform molecular viscosity is assumed within turbulent regions of any particular cell but, for liquids or even gaseous flows involving a large temperature range, significant variation in this property may occur across the sublayer. Our choices for such a situation are explained in Section 3.5.

3.2. Thermal analytical wall function

The analysis begins with the thermal field as, in the case of buoyant flows, the temperature enters the momentum equation as a source term and so needs to be determined first. On neglecting diffusion parallel to the wall the enthalpy transport equation may be written as

$$\rho U\frac{\partial T}{\partial x}+\rho V\frac{\partial T}{\partial y}=\frac{\partial}{\partial y}\left[\left(\frac{\mu}{Pr}+\frac{\mu_t}{Pr_t}\right)\frac{\partial T}{\partial y}\right], \tag{3.2}$$

or, in y^* coordinates

$$\frac{\partial}{\partial y^*}\left[\left(\frac{\mu}{Pr}+\frac{\mu_t}{Pr_t}\right)\frac{\partial T}{\partial y^*}\right]=\frac{\mu_v^2}{\rho_v^2 k_P}\left(\rho U\frac{\partial T}{\partial x}+\rho V\frac{\partial T}{\partial y}\right)=C_{th}. \tag{3.3}$$

The rationale of wall functions usually leads to convective transport being discarded on the grounds that near the wall it is negligible in comparison with diffusive transport. In the present work several different discretization strategies for including the main elements of the convective terms have been tried. The only stable approach was to retain just the first term in non-conservative form, i.e.,

$$C_{th}=\frac{\mu_v^2}{\rho_v^2 k_P}\left(\rho U\frac{\partial T}{\partial x}\right). \tag{3.4}$$

If we regard C_{th} as constant across the sublayer we may integrate Eq. (3.3) separately over the viscous and turbulent regions with continuity of T and $\partial T/\partial y^*$ imposed at the interface $y^*=y_v^*$. This results in the following expression for T:

$$T=\begin{cases} T_{wall}+\frac{Pr}{\mu_v}\left[\frac{C_{th}y^{*2}}{2}+A_{th}y^*\right], & y^*<y_v^*,\\ T_{wall}+\frac{Pr}{\mu_v\alpha_t}C_{th}(y^*-y_v^*) & \\ \quad+\frac{Pr}{\mu_v\alpha_t}\left[A_{th}+C_{th}\left(y_v^*-\frac{1}{\alpha_t}\right)\right]\ln Y_T & \\ \quad+\frac{Pry_v^*}{\mu_v}\left[\frac{C_{th}}{2}y_v^*+A_{th}\right], & y^*>y_v^*, \end{cases} \tag{3.5}$$

where $\alpha_t\equiv Pr\,\alpha/Pr_t$; $Y_T\equiv[1+\alpha_t(y^*-y_v^*)]$; $A_{th}\equiv -q_{wall}\mu_v/c_p\rho_v\sqrt{k_P}$.

3.3. Wall function for the velocity field

Following a similar path to the above analysis and notation, the velocity variation in the near-wall control volume is described by

$$\frac{\partial}{\partial y^*}\left[(\mu+\mu_t)\frac{\partial U}{\partial y^*}\right]=C+b(T-T_{ref}), \tag{3.6}$$

where

$$C\equiv\frac{\mu_v^2}{\rho_v^2 k_P}\left[\rho U\frac{\partial U}{\partial x}+\frac{\partial P}{\partial x}\right] \tag{3.7}$$

and $b\equiv-\mu_v^2/(\rho_v^2 k_P)\rho_{ref}g\beta$ represents the effect of buoyancy on the mean velocity with β being the coefficient of thermal expansion.

The equation is again integrated separately across the viscous and fully turbulent regions, resulting in analytical formulations for U, which can be used to compute the wall shear stress, given the value of U at the north face of the control volume, U_n. In our initial implementation of this approach, during the integration of the momentum equation (3.6), the variation of temperature T across the control volume was obtained from the analytical solutions given by Eq. (3.5) for the viscous and fully turbulent layers. The resulting expressions were, however, rather complex, and so the analytical temperature variation was subsequently approximated by a piecewise linear variation across the two regions. The temperature is first assumed to vary linearly across the viscosity-affected layer, between its wall value, T_{wall}, and the value resulting from the analytical solution, T_v. Across the fully turbulent region the temperature is then assumed to vary linearly between T_v and the temperature at the north face of the cell, T_n. This approximation leads to considerable simplifications in the analytical solution of the momentum equation without any detectable changes in the predictions. The details of the resulting functions are given in Appendices A and B.

In the case of buoyancy-affected flows, solution of the discretized momentum equation in the near-wall cell also requires a source term representing the average contribution of the buoyancy term across the cell:

$$\overline{F_B}=\frac{1}{y_n}\int_0^{y_n}\rho g\beta(T-T_{ref})\,dy. \tag{3.8}$$

In the present approach this can be evaluated by integrating the analytical temperature profiles described above, and the result is again given in Appendices A and B.

3.4. Mean dissipation rate and determination of y_v^*

The solution of the k equation over the near-wall cell requires one to compute the average generation and dissipation rates across the cell. The former can be evaluated by making use of the assumed turbulent viscosity variation and by obtaining $\partial U/\partial y$ from the analytical formulation obtained for the velocity in the fully turbulent part of the cell. For the average dissipation rate Chieng and Launder (1980) had assumed the following two-part dissipation profile across the wall adjacent cell. In the turbulent region the usual inverse dependence on distance was adopted:

$$\varepsilon=\frac{k_P^{3/2}}{c_l y} \tag{3.9}$$

and in the viscous layer we take the uniform limiting value

$$\varepsilon=\frac{2\nu k_P}{y_v^2} \tag{3.10}$$

motivated by the exact analytical result that, at the wall, $\varepsilon=\nu(\partial k^{1/2}/\partial y)^2\simeq 2\nu k/y^2$, Jones and Launder (1972). This proposal, shown in Fig. 3(a), pre-dated all the DNS results from the last 15 years which showed that, far from falling to the wall value as the experimental data available in the late 1970s had indicated, the maximum

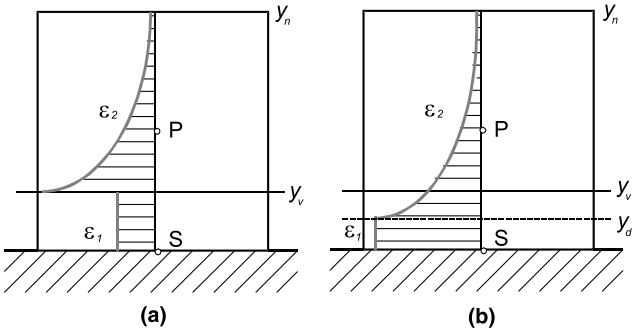

Fig. 3. Dissipation rate distribution for: (a) the standard and (b) the proposed wall function.

value of ε was found at the wall! Thus, to enable our model to accord with this observation, the inverse variation of ε with wall distance is continued closer to the wall, Fig. 3(b), to a position y_d selected so that there is no discontinuity of ε at the matching point: i.e.,

$$\frac{k_P^{3/2}}{c_l y_d} = \frac{2\nu k_P}{y_d^2}$$

or

$$y_d^* = 2c_l = 5.1. \tag{3.11}$$

The mean dissipation rate over this near-wall volume is then obtained by integrating this two-part variation to obtain

$$\overline{\varepsilon} = \frac{1}{y_n}\left[\frac{2k_P^{3/2}}{y_d^*} + \frac{k_P^{3/2}}{2.55}\ln\left(\frac{y_n}{y_d}\right)\right]. \tag{3.12}$$

There now remains only one additional constant to be fixed, namely the value of y_v^*. This is determined through numerical experiments for fully developed pipe flows, as 10.8. This adoption of different thicknesses for the viscous and dissipation sublayers not only brings the dissipation profile much closer to the distributions obtained in DNS studies; it also improves the prediction of the log law in forced convection. Qualitatively this choice of y_d smaller than y_v is also in accord with that made by Wolfshtein (1969) in his one-equation turbulence model.

3.5. Temperature dependence of viscosity

The variation of molecular viscosity with temperature means that in flows with significant heating some account of this temperature dependence will have to be made across the viscous sublayer, Fig. 2(b). Our initial strategy was to adopt a linear variation of molecular viscosity over this sub-region. The analytical integration of the momentum and enthalpy equations could still be carried out, but we were not successful in obtaining stable numerical solutions. Further analysis showed that the assumed linear variation could lead to a singularity. Accordingly, the linear variation of viscosity was replaced by a hyperbolic formula:

$$\mu = \frac{\mu_v}{1 + b_\mu(y^* - y_v^*)}, \quad 0 < y^* < y_v^*, \tag{3.13}$$

where $b_\mu = (\mu_{wall} - \mu_v)/\mu_{wall} y_v^*$. The form chosen gave a variation of $\mu(T)$ very close to the linear one, but without the stability problems.

3.6. Inclusion of laminarization effects

It has been well established since the mid-1960s that, if the shear stress decreases so rapidly with normal distance that the stress at the edge of the viscous layer is 10% or more below that of the wall, the viscous sublayer thickness y_v^* increases, leading to a marked reduction in the Nusselt number. Many simple mixing-length and one-equation models adopt empirical corrections that make the viscous layer thickness dependent on such factors as pressure gradient or wall suction rate (which were the agencies causing the decrease in shear stress in the cases under study). The wall-function treatment of Johnson and Launder (1982) also proposed including such an effect.

The same practice was initially followed in the present study. However, consistency would require that the turbulence energy, appearing in y_v^* should be evaluated at y_v, necessitating extrapolation of the values of k at y_P and y_N, a practice which, as noted above, was endemically unstable. Accordingly, some more stable adjustment which would nevertheless bring about the same effect was sought. The practice adopted was to adjust the mean level of turbulence energy dissipation in the near-wall cell. The factor by which $\overline{\varepsilon}$ was altered (F_ε) was to be made a function of an appropriate flow parameter. A dozen alternatives were tested but the one exhibiting least grid dependence and a satisfactory insensitivity to changes in Reynolds number was the ratio of shear stress at the edge of the viscous region to that at the wall. This ratio was subsequently modified to the generalized dimensionless parameter λ shown below:

$$\lambda = \left\{\left\{\mu_w\sqrt{\left(\frac{\partial U_i}{\partial x_j}\right)_w\left(\frac{\partial U_i}{\partial x_j}\right)_w}\right\} \Big/ \left\{\mu_v\sqrt{\left(\frac{\partial U_i}{\partial x_j}\right)_v\left(\frac{\partial U_i}{\partial x_j}\right)_v}\right\}\right\}. \tag{3.14}$$

The variation of the dimensionless thickness of the viscous inner region was then modelled by adjusting the average dissipation rate of turbulence over the near-wall control volume, through

$$\overline{\varepsilon}_{new} = F_\varepsilon \overline{\varepsilon}_{original}, \tag{3.15}$$

where

$$F_\varepsilon = \begin{cases} 1. + 1.5\{1 - \exp[-6.9(\lambda - 0.98)]\} \\ \quad \times\{1 - \exp[-193(\max(\alpha, 0))^2]\}, & \lambda \geqslant 1.0, \\ 1 - (1 - F_{\varepsilon o})\left[1 - \exp\left(-\frac{1-\lambda}{\lambda}\right)\right] \\ \quad \times\{1 - \exp[-11.1(\max(\gamma, 0))^2]\}, & \lambda < 1.0 \end{cases} \tag{3.16}$$

with

$$\alpha = \frac{\lambda}{1.02} - 1; \quad \gamma = \frac{0.98}{\lambda} - 1; \quad F_{\varepsilon o} = 0.75.$$

The above correlation was arrived at by determining the value of F_ε required to bring close agreement with the low-Reynolds number predictions of the k–ε model for mixed and forced convection in a pipe.

3.7. Other refinements

The form of the wall function presented did not (in contrast to earlier proposed versions) suffer greatly from grid dependence. However, when the viscous sublayer y_v occupied most or the whole of the near-wall control volume two steps were found desirable. Firstly, low-Reynolds number terms were included in the form of the k–ε model used in the external domain (that is, beyond the wall-adjacent cells). Secondly, when y_v becomes equal to or greater than y_n, the wall functions need to be based on an analysis where the viscous region occupies all of the control volume. The details are given in Gerasimov (2001). These treatments are included in the predictions shown in Figs. 10 and 11.

A further refinement introduced, which marks a departure from the conventional wall-function methodology, relates to the evaluation of the wall-parallel convective fluxes (in this case C_e and C_w) across the faces of the near-wall control volumes. In the conventional wall-function strategies, these fluxes are evaluated as in internal control volumes, by assuming that, as shown in Fig. 4(a), the flow variables remain constant over each cell face normal to the wall. Here we adopt the approach shown in Fig. 4(b), in which the convective flux is obtained by integrating the distribution of the flow variable obtained from the analytical solution.

Referring to Fig. 4, with the conventional wall function approach, the wall-parallel flux C_e, for the U-momentum is obtained from

$$C_e = \rho U_e, \quad \text{where } U_e = \frac{1}{2}(U_P + U_E)$$

in the present approach:

$$C_e = \frac{\rho}{U_e}\int_{y=0}^{y_n} U_{\text{an}_e}^2 \, \mathrm{d}y,$$

where U_e is as before and U_{an_e} is the analytical velocity profile at the control volume's east face.

This refinement was found to be especially beneficial to the prediction of the opposed wall jet and is likely to lead to similar predictive improvements in flows involving impingement and separation.

4. Implementation of the analytical wall function

The development of this new wall-function strategy has taken place within a structured, finite-volume flow solver, based on the SIMPLE pressure correction method. The implementation described here is therefore related to this numerical framework, though there is no reason why these concepts cannot be applied to flow solvers based on other methodologies.

4.1. Viscosity variations

The turbulent viscosity variation for $y^* > y_v^*$ is given by

$$\mu_t = \mu_v \alpha (y^* - y_v^*),$$

where μ_v is the molecular viscosity at y_v;

$$\alpha = c_\mu c_l, \quad y_v^* = 10.8.$$

The variation of molecular viscosity within the layer of zero turbulent viscosity $y^* < y_v^*$ is fitted to the following hyperbolic relation:

$$\mu = \frac{\mu_v}{1 + b_\mu (y^* - y_v^*)} \quad \text{with } b_\mu = \frac{\mu_{\text{wall}} - \mu_v}{y_v^* \mu_{\text{wall}}},$$

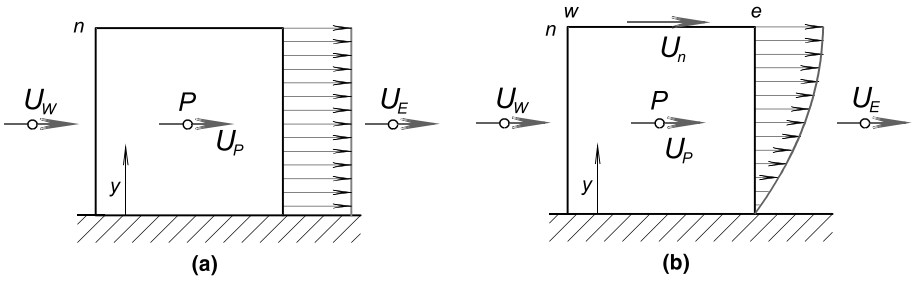

Fig. 4. (a) Uniform distribution. (b) Analytical distribution.

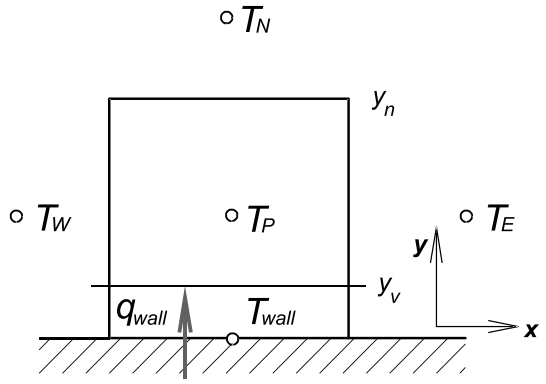

Fig. 5. Near-wall cell arrangement for thermal analytical wall function.

where μ_{wall} is the molecular viscosity at the wall temperature; μ_{v} is the molecular viscosity at the temperature T_{v} at y_{v}, obtained from the analytical solution. Note that for flows with constant molecular viscosity, $b_\mu = 0$.

4.2. Temperature wall function

The thermal convective transport, Eq. (3.4), over a near-wall control volume, Fig. 5, is normally approximated as

$$C_{\text{th}} = \frac{\mu_{\text{v}}^2}{\rho_{\text{v}}^2 k_P}\left(\rho_P U_P \frac{T_E - T_W}{x_E - x_W}\right). \tag{4.1}$$

An upwind approximation for $\mathrm{d}T/\mathrm{d}x$ can also be used.

The wall heat flux or wall temperature is obtained from one of the following:

Constant wall heat flux q_{wall}:

$$A_{\text{th}} = -\frac{q_{\text{wall}}}{c_p}\frac{\mu_{\text{v}}}{\rho_{\text{v}}\sqrt{k_P}}. \tag{4.2}$$

When $y_{\text{n}}^* > y_{\text{v}}^*$: T_{wall} is obtained from Eq. (A.4).
When $y_{\text{n}}^* < y_{\text{v}}^*$: T_{wall} is obtained from Eq. (B.4).

Constant wall temperature T_{wall}:

$$q_{\text{wall}} = -\frac{\rho_{\text{v}} c_p \sqrt{k_P}}{\mu_{\text{v}}} A_{\text{th}}. \tag{4.3}$$

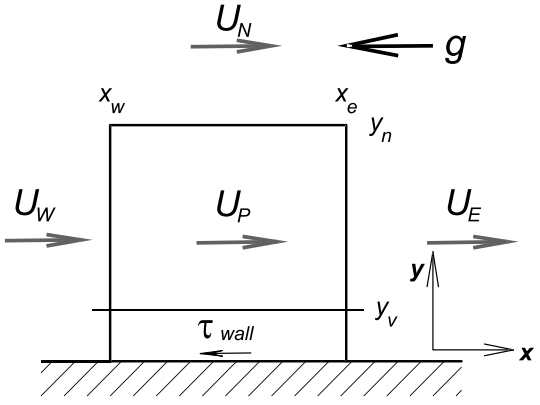

Fig. 6. Near-wall cell arrangement for hydrodynamic analytical wall function.

When $y_{\text{n}}^* > y_{\text{v}}^*$: A_{th} is obtained from Eq. (A.5).
When $y_{\text{n}}^* < y_{\text{v}}^*$: A_{th} is obtained from Eq. (B.5).

4.3. The velocity wall function

The quantity C defined by Eq. (3.7) is represented in finite-volume form as

$$C = \frac{\mu_{\text{v}}^2}{\rho_{\text{v}}^2 k_P}\left(\rho_P U_P \frac{U_E - U_W}{x_E - x_W} + \frac{P_e - P_w}{x_e - x_w}\right). \tag{4.4}$$

As with the temperature wall function, an upwind approximation for $\mathrm{d}U/\mathrm{d}x$ can also be used.

The wall shear stress τ_{wall}, Fig. 6, is obtained from

$$\tau_{\text{wall}} = -\frac{\rho_{\text{v}}\sqrt{k_P}}{\mu_{\text{v}}} A_1. \tag{4.5}$$

When $y_{\text{n}}^* > y_{\text{v}}^*$: A_1 is obtained from Eqs. (A.11) and (A.12). The buoyant force term over the near-wall control volume P, is obtained from Eq. (A.14).

When $y_{\text{n}}^* < y_{\text{v}}^*$: A_1 is obtained from Eqs. (B.8) and (B.5). The buoyant force term over the near-wall control volume P, is obtained from Eq. (B.11).

4.4. Wall function for turbulent kinetic energy, k

Since k varies as y^2 in the immediate vicinity of the wall the molecular diffusion of turbulent energy to the wall is zero.

The average production rate of k over the near-wall control volume is obtained from

$$P_k = \frac{1}{y_{\text{n}}}\frac{\rho_{\text{v}}\sqrt{k_P}}{\mu_{\text{v}}}\int_{y_{\text{v}}^*}^{y_{\text{n}}^*} \mu_{\text{v}}\alpha(y^* - y_{\text{v}}^*)\left(\frac{\partial U}{\partial y^*}\right)^2 \mathrm{d}y^*, \tag{4.6}$$

where $\partial U/\partial y^*$ is obtained from Eq. (A.17). Here the above expression was integrated numerically. In isothermal flows, where $b = b_\mu = 0$, Eq. (A.17) becomes simple enough for the above equation to be integrated analytically. Also it is worth noting that when $y_{\text{n}}^* < y_{\text{v}}^*$, $P_k = 0$).

The average dissipation rate of k over the near-wall control volume is obtained as follows (see Fig. 7):

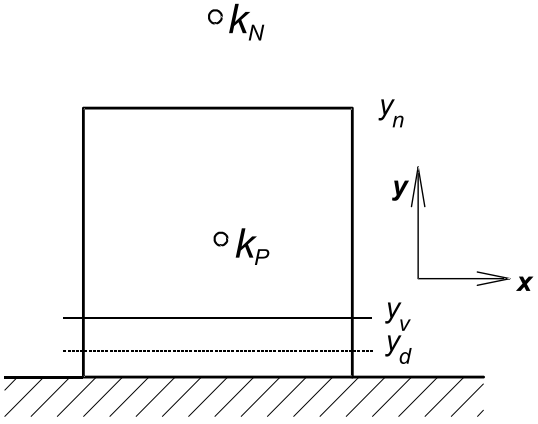

Fig. 7. Near-wall cell arrangement showing y_{v} and y_{d} thicknesses.

For $y_n^* > y_d^*$:

$$\overline{\varepsilon} = \frac{F_\varepsilon}{y_n}\left[\frac{2k_P^{3/2}}{y_d^*} + \frac{k_P^{3/2}}{2.55}\ln\left(\frac{y_n}{y_d}\right)\right]. \tag{4.7}$$

For $y_n^* < y_v^*$: $F_\varepsilon = 1$.

For $y_n^* > y_v^*$: F_ε is obtained from Eqs. (3.14) and (3.16) in Section 3.6.

For $y_n^* < y_d^*$:

$$\overline{\varepsilon} = \frac{2\nu k_P}{y_d^2}. \tag{4.8}$$

4.5. Wall function for dissipation rate ε

As in the conventional wall function approaches, the transport equation for ε is not integrated over the near-wall control volume. The nodal value of ε at the near-wall control volumes ε_P is prescribed as follows:

$$\varepsilon_P = F_\varepsilon \frac{k_P^{3/2}}{c_l y_P}. \tag{4.9}$$

This value is needed to represent the slope of ε normal to the wall at the north face of the control volume.

5. Applications of wall functions

Three test cases have been examined to date

- Fully developed flow in a pipe.
- Mixed convection flow in a vertical pipe where buoyancy due to the heated pipe wall is aiding the forced flow.
- The opposed two-dimensional wall jet.

In all cases considerable care was taken to ensure that the results were independent of the grid used in the main part of the flow. The grids used consisted of 15 nodes for the fully developed pipe flow, 127 by 15 axial and radial nodes, respectively, for the mixed convection flow and 102 by 280 nodes for the opposed wall jet flow. The sensitivity of the results to the thickness of the wall-adjacent cells was one of the test criteria that discriminated between alternative near-wall treatments.

For the first two cases above results have been obtained for four different thicknesses of the wall-adjacent cells over a 15-fold range of bulk Reynolds number and, for the second case, under different buoyancy-driven conditions. The mean velocity profile in conventional wall-law coordinates is shown in Figs. 8 and 9 for two Reynolds numbers. At a Reynolds number of 10^5 we note that the velocity close to the wall falls on the log-law line $U^+ = 2.4\ln y^+ + 5.45$ irrespective of the thickness of the near-wall cell. The near-wall cell thickness y_n^* is roughly three times the corresponding value of y_n^+. Thus, it will be appreciated that for the smallest value of y_n^* most of the near-wall cell lies in the viscous sublayer. It is known that when the bulk Reynolds number falls below 10^4 the additive constant in the log-law relationship increases as the Reynolds number is lowered. Fig. 9

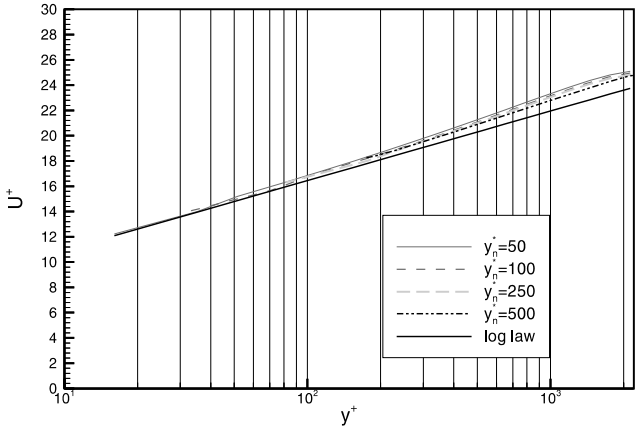

Fig. 8. Semi-logarithmic velocity profiles for $Re = 100,000$ for isothermal fully developed pipe flow.

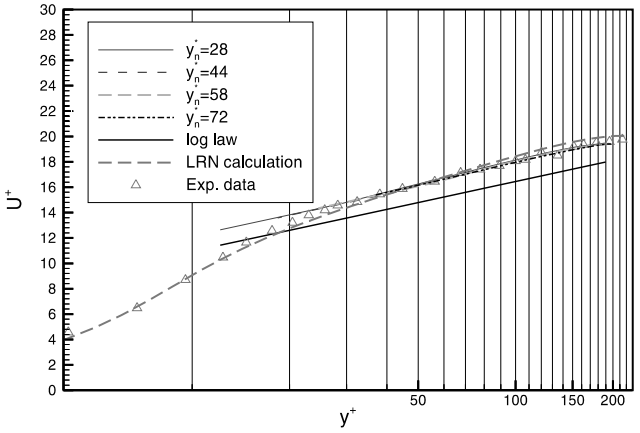

Fig. 9. Semi-logarithmical velocity profiles for $Re = 6753$ for isothermal fully developed pipe flow.

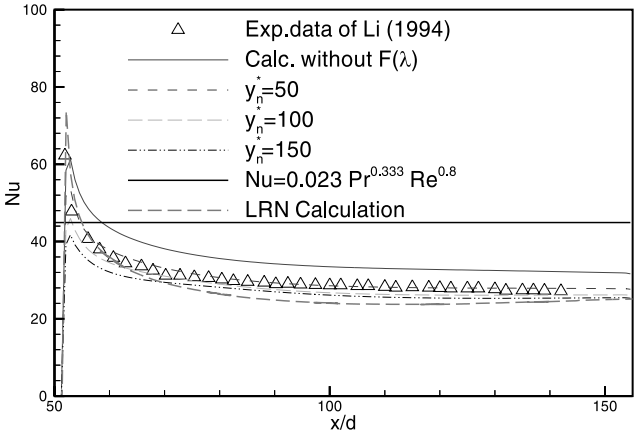

Fig. 10. Predicted Nusselt number for mixed convection at $Re = 15,000$ and $Gr = 2.2 \times 10^8$ in upward flow in a heated pipe.

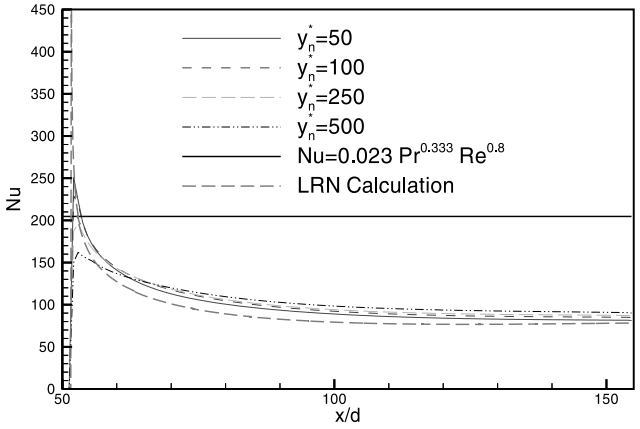

Fig. 11. Predicted Nusselt number for mixed convection at $Re = 100,000$ and $Gr = 3.5 \times 10^9$ in upward flow in a heated pipe.

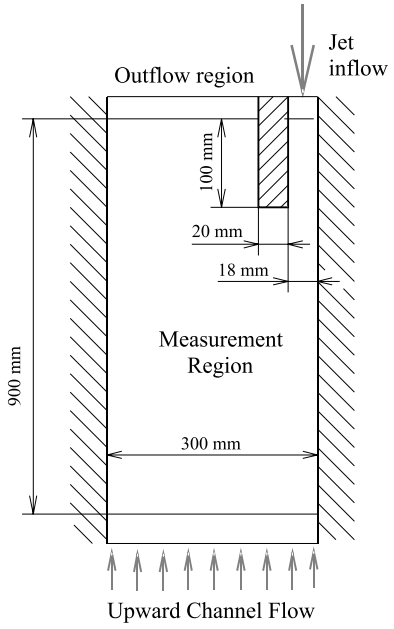

Fig. 12. Opposed water jet. Jet flow rate $\dot{m}_{jet} = 3.03$ kg/s; upward flow rate $\dot{m}_{up} = 3.88$ kg/s; channel depth = 1.2 m.

shows the experimental data of Kudva and Sesonske (1972) for $Re = 6753$ with which the low-Reynolds-number k–ε model of Launder and Sharma (1974) is in very close accord. For present purposes, however, the point of interest is that, with the new wall functions, good agreement is also obtained, including the displacement of the velocity profile above the "universal" log-law.

Fig. 10 relates to mixed convection in a vertical pipe for an inlet bulk Reynolds number of 15,000 and a Grashof number ($Gr_d = g\beta d^4 q_{wall}/v^2 k$) value of 2.163×10^8. Entry conditions correspond to those of isothermal fully developed flow. Thermal boundary conditions of uniform wall heat flux are imposed. Due to the wall heating, the near-wall fluid receives a buoyant upthrust, causing a local velocity maximum and a rapid decrease of shear stress with distance from the wall. This leads to

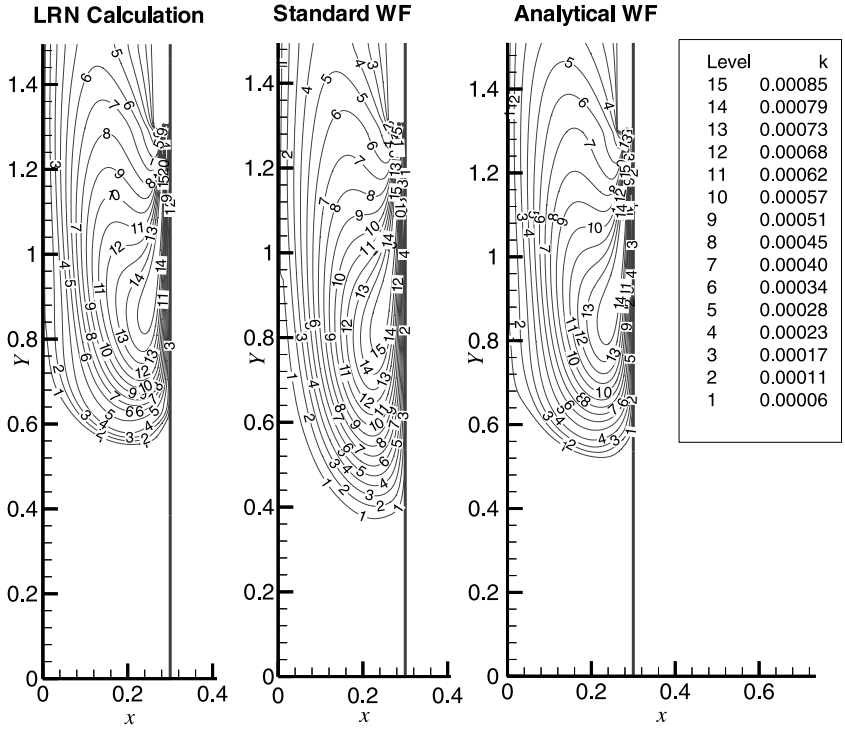

Fig. 13. Predicted distribution of the turbulent kinetic energy by Standard WF, Analytical WF and Launder–Sharma LRN k–ε model in downward-directed opposed wall jet; x and y in meters, k in m^2/s^2.

a thickening of the viscous sublayer and a reduction of Nusselt number below that found in fully developed, forced convection pipe flow at the same Reynolds number (denoted by the horizontal line in Fig. 10, the Dittus–Boelter correlation). The success of the low-Reynolds number k–ε model in predicting such flows was first shown by Cotton and Jackson (1987). The development of the data of Li (1994) accords with the above description. Moreover, we see that not only the low-Reynolds number model but also the various wall-function computations are in excellent agreement with the experimental data. It is noted that for one set of calculations the sublayer thickening was switched off leading to a significant rise in Nusselt number. However, it is equally clear that this is just one of the factors contributing to the reduction of Nusselt number.

The close agreement that the wall functions give with the low-Reynolds number predictions has been verified over a far wider range of conditions than those for which experiments exist. Fig. 11 shows, for example, a situation at an inlet Reynolds number of nearly 10^5 and $Gr_d = 3.49 \times 10^9$, where, due to the strong heating, the Nusselt number is reduced to only 40% of that found for purely forced convection. Again the agreement of the wall-function results with the low-Reynolds number model is impressively close.

The final test case is an isothermal, downward directed wall jet shown in Fig. 12, which was measured by Jackson et al. (2000). This is a preliminary test case for future applications where the wall jet will be significantly hotter than the very slow moving upward bulk flow. In all the computations, standard wall functions have been used on the left-hand wall. Thus Fig. 13 shows purely the effect of using different treatments along the right-hand wall downstream from the jet inflow. The results with the standard wall functions show the jet to penetrate further than when using the low-Reynolds number k–ε model. The contours of turbulent kinetic energy obtained with the new analytical wall functions, on the other hand, are considerably closer to those of the low-Reynolds number model than is achieved by the standard wall-function prescription.

6. Concluding remarks

The present analytical wall functions, termed the UMIST-A scheme, [1] have achieved a significant broadening of the range of near-wall turbulent flows that can be satisfactorily resolved with wall functions. Use of the scheme described above reduces the overall computing time required by between one and two orders of magnitude compared with a conventional low-Reynolds number model.

For the first time it is possible to compute mixed as well as forced-convection flows with wall functions and the sensitivity of the results to the size of the near-wall cell has also been greatly reduced. In a separate programme of testing, to be reported elsewhere, Robinson (2001) has shown that the scheme also improves the prediction of stalled flow in a diffuser.

In closing, it is as well to note flow situations that the approach is either not well suited to modelling or where some adaptation to the present method is needed. In the latter area, the assumption that the velocity and thermal sublayer thicknesses are the same probably means that the accuracy will deteriorate for Prandtl numbers much greater than or much less than unity. Thus it would be desirable to prescribe the ratio of the thicknesses of the thermal to velocity sublayers as a function of molecular Prandtl number. Less easily rectified are situations where the near-wall velocity vector undergoes appreciable skewing very close to the wall, i.e., within the wall function region. Our current view is that a *numerical* treatment of this sublayer region is then preferable, an approach (UMIST-N) documented in Craft et al. (2001).

Acknowledgements

Financial support for the work has been coordinated by British Energy plc through contract no. BWD40029343. AVG acknowledges also the support of a UK ORS scholarship. Authors' names are listed alphabetically.

Appendix A. Wall function formulae

Molecular viscosity variation

$$\mu = \frac{\mu_v}{1 + b_\mu (y^* - y_v^*)}, \quad \text{where } b_\mu = \frac{\mu_{wall} - \mu_v}{\mu_{wall} y_v^*}.$$

Turbulent viscosity variation

$$\mu_t = \mu_v \alpha (y^* - y_v^*), \quad \text{where } \alpha = c_\mu c_l.$$

Constant b_μ should be set equal to zero if the variation of fluid properties across the viscous sublayer is negligible.

A.1. Thermal analytical wall function

In the viscous sublayer ($y^* < y_v^*$)

$$T_l = \frac{Pr}{\mu_v}\left[\frac{C_{th} y^{*2}}{2} + A_{th} y^*\right] + \frac{Pr b_\mu}{\mu_v}\left[\frac{C_{th} y^{*3}}{3} - \frac{C_{th} y_v^* - A_{th}}{2} y^{*2} - A_{th} y_v^* y^*\right] + T_{wall}. \quad \text{(A.1)}$$

[1] UMIST: Unified Modelling via Integrated Sublayer Transport; A denotes analytical.

In the fully turbulent region ($y^* > y_v^*$)

$$T_2 = \frac{Pr}{\mu_v \alpha_t} C_{th}(y^* - y_v^*) + \frac{Pr}{\mu_v \alpha_t}\left[A_{th} + C_{th}\left(y_v^* - \frac{1}{\alpha_t}\right)\right] \ln Y_T + \frac{Pr y_v^*}{\mu_v}\left[\frac{C_{th}}{2} y_v^* + A_{th}\right] - b_\mu \frac{Pr y_v^{*2}}{2\mu_v}\left[\frac{C_{th}}{3} y_v^* + A_{th}\right] + T_{wall}, \tag{A.2}$$

where

$$Y_T = [1 + \alpha_t(y^* - y_v^*)]; \quad \alpha_t = \frac{Pr\alpha}{Pr_t}.$$

For prescribed wall heat flux boundary conditions, q_{wall}:

$$A_{th} = -\frac{q_{wall}}{c_p} \frac{\mu_v}{\rho_v \sqrt{k_P}}. \tag{A.3}$$

Expression for the wall temperature

$$T_{wall} = T_n - \frac{Pr}{\mu_v}\left\{\frac{C_{th}}{\alpha_t}(y_n^* - y_v^*) + \frac{\ln Y_{Tn}}{\alpha_t}\left[A_{th} + C_{th}\left(y_v^* - \frac{1}{\alpha_t}\right)\right] + y_v^*\left(A_{th} + \frac{C_{th} y_v^*}{2}\right)\right\} + b_\mu \frac{Pr y_v^{*2}}{2\mu_v}\left[\frac{C_{th} y_v^*}{3} + A_{th}\right], \tag{A.4}$$

where

$$Y_{Tn} = [1 + \alpha_t(y_n^* - y_v^*)].$$

For prescribed wall temperature T_{wall}:

$$A_{th1} = \left\{(T_n - T_{wall})(\mu_v/Pr) - (1/\alpha_t)C_{th}(y_n^* - y_v^*) - (C_{th}/\alpha_t)\left(y_v^* - \frac{1}{\alpha_t}\right)\ln Y_{Tn} - (C_{th}/2)y_v^{*2} + b_\mu(C_{th} y_v^{*3}/6)\right\} \Big/ \left\{(1/\alpha_t)Y_{Tn} + y_v^* - (1/2)b_\mu y_v^{*2}\right\}, \tag{A.5}$$

$$q_{wall} = -\frac{\rho_v c_p \sqrt{k_P}}{\mu_v} A_{th}. \tag{A.6}$$

A.2. Hydrodynamic analytical wall function for buoyant flows

Expression for the velocity within the viscous sublayer ($y^* < y_v^*$)

$$\mu_v U_1 = \frac{C}{2} y^{*2} + A_1 y^* + \frac{b}{2}(T_{wall} - T_{ref}) y^{*2} - \frac{b}{6 y_v^*}(T_{wall} - T_v) y^{*3} + b b_\mu y^{*2}(T_{wall} - T_{ref}) \times \left(\frac{y^*}{3} - \frac{y_v^*}{2}\right) - \frac{b b_\mu}{2 y_v^*} y^{*3}(T_{wall} - T_v)\left(\frac{y^*}{4} - \frac{y_v^*}{3}\right) + b_\mu C y^{*2}\left(\frac{y^*}{3} - \frac{y_v^*}{2}\right) + b_\mu A_1 y^*\left(\frac{y^*}{2} - y_v^*\right), \tag{A.7}$$

where constant $b \equiv -(v_v^2/k_P)\rho_{ref} g\beta$ represents the effect of buoyancy on the mean velocity with β being the coefficient of thermal expansion. The wall functions can be appreciably simplified in pure forced convection. In this case all terms containing the b constant should be omitted in order to neglect the effect of buoyancy. In the fully turbulent region ($y^* > y_v^*$):

$$\mu_v U_2 = \frac{C}{\alpha}\left[y^* - \left(\frac{1}{\alpha} - y_v^*\right)\ln Y\right] + \frac{A_2}{\alpha}\ln Y + b\frac{(T_v - T_{ref} + \delta T_y y_v^*)}{\alpha}\left[y^* - \left(\frac{1}{\alpha} - y_v^*\right)\ln Y\right] - b\frac{\delta T_y}{2\alpha}\left[\frac{y^{*2}}{2} - y^*\left(\frac{1}{\alpha} - y_v^*\right) + \left(\frac{1}{\alpha} - y_v^*\right)^2 \ln Y\right] + B_2, \tag{A.8}$$

where

$$Y = [1 + \alpha(y^* - y_v^*)]; \quad \delta T_y = \frac{T_v - T_n}{y_n^* - y_v^*},$$

$$B_2 = y_v^* C\left(\frac{y_v^*}{2} - \frac{1}{\alpha}\right) + A_1 y_v^* + b\frac{y_v^{*2}}{2}\left[\frac{2T_{wall} + T_v}{3} - T_{ref}\right] - \frac{b y_v^*}{\alpha}\left[T_v - T_{ref} + \frac{1}{2}\left(\frac{y_v^*}{2} + \frac{1}{\alpha}\right)\frac{T_v - T_n}{y_n^* - y_v^*}\right] - b b_\mu \frac{y_v^{*3}}{6}\left[\frac{3T_{wall} + T_v}{4} - T_{ref}\right] - b_\mu \frac{y_v^{*2}}{2}\left(\frac{C}{3} y_v^* + A_1\right), \tag{A.9}$$

$$A_2 = b y_v^*\left[\frac{T_{wall} - T_v}{2} - \frac{T_v - T_n}{y_n^* - y_v^*}\frac{y_v^*}{2}\right] + A_1, \tag{A.10}$$

$$A_1 = \frac{\mu_v U_n - N}{\left[(\ln Y_n/\alpha) + y_v^* - b_\mu(y_v^{*2}/2)\right]}, \tag{A.11}$$

$$N = \frac{C}{\alpha}\left[y_n^* - y_v^* - \left(\frac{1}{\alpha} - y_v^*\right)\ln Y_n + \frac{\alpha y_v^{*2}}{2}\right] + \frac{b y_v^*}{\alpha}\left[\frac{T_{wall} - T_v}{2}\ln Y_n - (T_v - T_{ref})\right] + b\frac{(T_v - T_{ref} + \delta T_y y_v^*)}{\alpha}\left[y_n^* - \left(\frac{1}{\alpha} - y_v^*\right)\ln Y_n\right] - b\frac{\delta T_y}{2\alpha}\left\{\frac{(y_n^* + y_v^*)^2}{2} - \frac{y_n^* - y_v^*}{\alpha} + \left[\left(\frac{1}{\alpha} - y_v^*\right)^2 + y_v^{*2}\right]\ln Y_n\right\} + b\frac{y_v^{*2}}{2}\left[\frac{2T_{wall} + T_v}{3} - T_{ref}\right] - b b_\mu \frac{y_v^{*3}}{6}\left[\frac{3T_{wall} + T_v}{4} - T_{ref}\right] - b_\mu \frac{y_v^{*3}}{6} C_1. \tag{A.12}$$

The expression for the shear stress:

$$\tau_{wall} = -\frac{\rho_v \sqrt{k_P}}{\mu_v} A_1. \tag{A.13}$$

The average buoyant term in the momentum equation can also be obtained analytically through integration, giving

$$\overline{F_b} = \beta'\left[\left(\frac{T_{\rm wall}+T_{\rm v}}{2}-T_{\rm ref}\right)y_{\rm v}^{*}+\left(\frac{T_{\rm v}+T_{\rm n}}{2}-T_{\rm ref}\right)(y_{\rm n}^{*}-y_{\rm v}^{*})\right] \tag{A.14}$$

with

$$\beta' = \frac{\rho_{\rm ref} g\beta\mu_{\rm v}}{y_{\rm n}\rho_{\rm v}\sqrt{k_P}}. \tag{A.15}$$

Average kinetic energy production

$$\overline{P_k} = \frac{1}{y_{\rm n}}\frac{\rho_{\rm v}\sqrt{k_P}}{\mu_{\rm v}}\int_{y_{\rm v}^{*}}^{y_{\rm n}^{*}}\mu_{\rm v}\alpha(y^{*}-y_{\rm v}^{*})\left(\frac{\partial U_2}{\partial y^{*}}\right)^2 {\rm d}y^{*}, \tag{A.16}$$

where

$$\frac{\partial U_2}{\partial y^{*}} = \frac{1}{\mu_{\rm v}Y}\left[Cy^{*}+A_2+b(T_{\rm v}-T_{\rm ref}+\delta T_y y_{\rm v}^{*})y^{*}-b\frac{\delta T_y}{2}y^{*2}\right]. \tag{A.17}$$

Appendix B. Wall-function approach for a case when the viscous sublayer becomes thicker than the near-wall cell ($y_{\rm n}^{*} < y_{\rm v}^{*}$)

Here Eqs. (3.3) and (3.6) with $\mu_{\rm t}=0$ are integrated across the entire near-wall control volume, with boundary conditions at $y=y_{\rm n}$: $U=U_{\rm n}$ and $T=T_{\rm n}$, respectively. Molecular viscosity variation

$$\mu = \frac{\mu_{\rm n}}{1+b_\mu(y^{*}-y_{\rm n}^{*})}, \quad \text{where } b_\mu = \frac{\mu_{\rm wall}-\mu_{\rm n}}{\mu_{\rm wall}y_{\rm n}^{*}}. \tag{B.1}$$

B.1. Thermal analytical wall function

$$T = \frac{Pr}{\mu_{\rm v}}\left[\frac{C_{\rm th}y^{*2}}{2}+A_{\rm th}y^{*}\right]+\frac{Pr\,b_\mu}{\mu_{\rm v}}\left[\frac{C_{\rm th}y^{*3}}{3}-\frac{C_{\rm th}y_{\rm n}^{*}-A_{\rm th}}{2}y^{*2}-A_{\rm th}y_{\rm n}^{*}y^{*}\right]+T_{\rm wall}. \tag{B.2}$$

For prescribed wall heat flux boundary conditions, $q_{\rm wall}$:

$$A_{\rm th} = -\frac{q_{\rm wall}}{c_p}\frac{\mu_{\rm n}}{\rho_{\rm n}\sqrt{k_P}}, \tag{B.3}$$

$$\begin{aligned}T_{\rm wall} &= T_{\rm n}-\frac{Pr\,y_{\rm n}^{*}}{\mu_{\rm n}}\left(\frac{C_{\rm th}y_{\rm n}^{*}}{2}+A_{\rm th}\right)+b_\mu\frac{Pr\,y_{\rm n}^{*2}}{2\mu_{\rm n}}\left[\frac{C_{\rm th}y_{\rm n}^{*}}{3}+A_{\rm th}\right]\\ &= T_{\rm n}-\frac{Pr\,C_{\rm th}y_{\rm n}^{*2}}{2\mu_{\rm n}}\left(1-b_\mu\frac{y_{\rm n}^{*}}{3}\right)+\frac{Pr\,y_{\rm n}q_{\rm wall}}{\mu_{\rm n}c_p}\left(1-b_\mu\frac{y_{\rm n}^{*}}{2}\right).\end{aligned} \tag{B.4}$$

For prescribed wall temperature $T_{\rm wall}$:

$$A_{\rm th1} = \frac{(T_{\rm n}-T_{\rm wall})(\mu_{\rm n}/Pr)-(C_{\rm th}/2)y_{\rm n}^{*2}+b_\mu(C_{\rm th}y_{\rm n}^{*3}/6)}{y_{\rm n}^{*}-(1/2)b_\mu y_{\rm n}^{*2}}, \tag{B.5}$$

$$\begin{aligned}q_{\rm wall} &= -\frac{\rho_{\rm n}c_p\sqrt{k_P}}{\mu_{\rm n}}A_{\rm th}\\ &= -\frac{c_p\left[(T_{\rm n}-T_{\rm wall})(\mu_{\rm n}/Pr)-(C_{\rm th}/2)y_{\rm n}^{*2}+b_\mu(C_{\rm th}y_{\rm n}^{*3}/6)\right]}{y_{\rm n}-(1/2)b_\mu y_{\rm n}y_{\rm n}^{*}}.\end{aligned} \tag{B.6}$$

B.2. Hydrodynamic analytical wall function for buoyant flows

Expression for the velocity

$$\begin{aligned}\mu_{\rm n}U = {}&\frac{C}{2}y^{*2}+A_1y^{*}+\frac{by^{*2}}{2}(T_{\rm wall}-T_{\rm ref})\\ &-\frac{b}{6y_{\rm n}^{*}}(T_{\rm wall}-T_{\rm v})y^{*3}+bb_\mu y^{*2}\left(\frac{y^{*}}{3}-\frac{y_{\rm n}^{*}}{2}\right)\\ &\times(T_{\rm wall}-T_{\rm ref})-\frac{bb_\mu}{2y_{\rm n}^{*}}y^{*3}\left(\frac{y^{*}}{4}-\frac{y_{\rm n}^{*}}{3}\right)(T_{\rm wall}-T_{\rm v})\\ &+b_\mu Cy^{*2}\left(\frac{y^{*}}{3}-\frac{y_{\rm n}^{*}}{2}\right)+b_\mu A_1y^{*}\left(\frac{y^{*}}{2}-y_{\rm n}^{*}\right),\end{aligned} \tag{B.7}$$

where

$$A_1 = \frac{\mu_{\rm n}U_{\rm n}-N}{y_{\rm n}^{*}-b_\mu(y_{\rm n}^{*2}/2)}, \tag{B.8}$$

$$\begin{aligned}N = {}&\frac{C}{2}y_{\rm n}^{*2}+\frac{by_{\rm n}^{*2}}{2}\left[\frac{2T_{\rm wall}+T_{\rm n}}{3}-T_{\rm ref}\right]\\ &-\frac{bb_\mu y_{\rm n}^{*3}}{6}\left[\frac{3T_{\rm wall}+T_{\rm n}}{4}-T_{\rm ref}\right]-\frac{b_\mu Cy_{\rm n}^{*3}}{6}.\end{aligned} \tag{B.9}$$

The expression for the shear stress:

$$\tau_{\rm wall} = -\frac{\rho_{\rm n}\sqrt{k_p}}{\mu_{\rm n}}A_1 = -\frac{\mu_{\rm n}U_{\rm n}-N}{y_{\rm n}-b_\mu(y_{\rm n}^{*}y_{\rm n}/2)}. \tag{B.10}$$

The average buoyant term in the momentum equation:

$$\overline{F_b} = \beta'\left[\left(\frac{T_{\rm wall}+T_{\rm n}}{2}-T_{\rm ref}\right)y_{\rm n}^{*}\right]. \tag{B.11}$$

Average kinetic energy production:

$$P_k = 0. \tag{B.12}$$

References

Chieng, C.C., Launder, B.E., 1980. On the calculation of turbulent heat transfer downstream from abrupt pipe expansion. Numer. Heat Transfer 3, 189–207.

Ciofalo, M., Collins, M.W., 1989. k–ε predictions of heat transfer in turbulent recirculating flows using an improved wall treatment. Int. J. Heat Mass Transfer B 15, 21–47.

Cotton, M.A., Jackson, J.D., 1987. Calculation of turbulent mixed convection in a vertical tube using a low-Reynolds number k–ε turbulence model. In: Proceedings of the 6th Symposium on Turbulent Shear Flows, Toulouse.

Craft, T.J., Gant, S.E., Iacovides, H., Launder, B.E., 2001. Development and application of a numerical wall-function strategy for complex near-wall flows. In: ECCOMAS CFD 2001 Conference, Swansea.

Gerasimov, A.V., 2001. Development of a new analytical wall-function approach for modelling mixed convection phenomena. Technical Report BWD 40029343, Mechanical Engineering Department, University of Manchester Institute of Science and Technology.

Jackson, J.D., He, S., Xu, Z., Wu, T., 2000. CFD quality and trust – generic studies of thermal convection. Technical Report HTH/GNSR/5029, School of Engineering, University of Manchester.

Johnson, R.W., Launder, B.E., 1982. Discussion of "On the calculation of turbulent heat transfer downstream from an abrupt pipe expansion". Numer. Heat Transfer 5, 493–496.

Jones, W.P., Launder, B.E., 1972. The prediction of laminarization with a two-equation model of turbulence. Int. J. Heat Mass Transfer 15, 301–314.

Kudva, A.A., Sesonske, A., 1972. Structure of turbulent velocity and temperature fields in ethylene glycol pipe flow at low Reynolds number. Int. J. Heat Mass Transfer 15, 127.

Launder, B.E., Sharma, B.I., 1974. Application of the energy-dissipation model of turbulence to the calculation of flow near a spinning disc. Lett. Heat Mass Transfer 1, 131–138.

Launder, B.E., Spalding, D.B., 1974. The numerical computation of turbulent flows. Comput. Meth. Appl. Mech. Engrg. 3, 269–289.

Li, J., 1994. Studies of buoyancy-influenced convective heat transfer to air in a vertical tube. Ph.D. Thesis, University of Manchester.

Patankar, S.V., Spalding, D.B., 1967. Heat and Mass Transfer in Boundary Layers. Morgan-Grampian Press, London.

Robinson, C., 2001. Advanced CFD modelling of road–vehicle aerodynamics. PhD thesis, UMIST.

Spalding, D.B., 1967. Monograph on turbulent boundary layers. Technical Report TWF/TN/33, Department of Mechanical Engineering, Imperial College of Science and Technology (Chapter 2).

Wolfshtein, M., 1969. The velocity and temperature distribution in one-dimensional flow with turbulence augmentation and pressure gradient. Int. J. Heat Mass Transfer 12, 301–318.